Subsurface Mixing Dynamics across the Salt-freshwater Interface

Kevin Y.L De Vriendt[1], Tanguy Le Borgne[2], Maria Pool[1], and Marco Dentz[1]

[1]IDAEA-CSIC
[2]Université de Rennes 1

November 24, 2022

Abstract

Mixing along the salt-freshwater interface is critical for geochemical reactions, transport and transformation of nutrients and contaminants in coastal ecosystems. However, the mechanisms and controls of mixing are not well understood. We develop an analytical model, based on the coupling between flow deformation and dispersion, that predicts the mixing dynamics along the interface for steady state flow in coastal aquifers. The analytical predictions are compared with the results of detailed numerical simulations, which show that non-uniform flow fields, inherent to seawater intrusion in coastal aquifer, result in a non-monotonic evolution of mixing width and mixing rates along the interface. The analytical model accurately captures these dynamics over a range of freshwater flow rates and dispersivities. It predicts the evolution of the mixing width and mixing rates along the interface, offering a new framework for understanding and modeling mixing and reaction processes in coastal aquifers.

Subsurface Mixing Dynamics across the Salt-freshwater Interface

K. De Vriendt[1],T. Le Borgne[2], M. Pool [2], M.Dentz [1]

[1]Institute of Environmental Assessment and Water Research, IDAEA-CSIC, 08034 Barcelona, Spain
[2]Université de Rennes 1, CNRS, Géosciences Rennes UMR 6118, Rennes, France
[3]AMPHOS 21 Consulting S. L., 08019 Barcelona

Key Points:

- The width of the saltwater-freshwater interface and mixing rate vary along the interface.
- Interface width and mixing dynamics are related through flow deformation.
- We derive an analytical model that predicts the mixing width and rate based on the interface profile and transverse dispersivity.

Corresponding author: Marco Dentz, `marco.dentz@csic.es`

Abstract

Mixing along the salt-freshwater interface is critical for geochemical reactions, transport and transformation of nutrients and contaminants in coastal ecosystems. However, the mechanisms and controls of mixing are not well understood. We develop an analytical model, based on the coupling between flow deformation and dispersion, that predicts the mixing dynamics along the interface for steady state flow in coastal aquifers. The analytical predictions are compared with the results of detailed numerical simulations, which show that non-uniform flow fields, inherent to seawater intrusion in coastal aquifer, result in a non-monotonic evolution of mixing width and mixing rates along the interface. The analytical model accurately captures these dynamics over a range of freshwater flow rates and dispersivities. It predicts the evolution of the mixing width and mixing rates along the interface, offering a new framework for understanding and modeling mixing and reaction processes in coastal aquifers.

Plain Language Summary

Density differences between salt and freshwater leads to the formation of a convection cell in coastal aquifers, in which seawater intrudes inland along the aquifer bottom. Fresh and mixed waters flow upwards along the salt-freshwater interface and are forced to accelerates before being discharged along the ocean seabed. The resulting non-uniform flow alters the concentration of the mixed waters along the interface, which in turn enhances mixing rates and creates local mixing hotspots. Our results show how non-uniform velocity fields result in enhanced local mixing dynamics, and elucidate the mechanisms and controls of mixing processes along salt-freshwater interfaces in coastal aquifers.

1 Introduction

Coastal aquifers are some of the most vulnerable groundwater resources sustaining dense coastal populations globally (Ferguson & Gleeson, 2012). These subsurface environments are subject to significant anthropogenic pollutants that negatively impact ocean ecosystems (Slomp & Cappellen, 2004; Moore, 2010; Kroeger & Charette, 2008). Moreover, their inherently non-stationary flow dynamics on different temporal scales (tides, seasons and glacial cycles) leads to a range of geochemical processes across coastal landscapes. A notable example is mixing-enhanced carbonate dissolution and karstification processes in coastal zones (Back et al., 1986a). Over large time scales, Seawater Intrusion has acted as primary mechanism to observable land features such as the formation of 'Flank Margin Caves' near the mixing discharge zone (Mylroie & Carew, 1990; Back et al., 1979), or cave and conduits formation in Bermudas (A. Palmer, 1992), Bahamas (R. Palmer & Williams, 1982) and Yucatán (Back et al., 1986b). Freshwater discharge in coastal aquifers has also been associated with a variety of other biogeochemical reactions in beach environments. A well-known example is the enhanced iron oxide precipitation in Waquiot Bay (termed 'iron curtain') (Charette & Sholkovitz, 2002; Spiteri et al., 2008) which attenuates contaminants such as phosphates and arsenic. Such reactions may hold a strong propensity in regulating the flux of terrestrial pollutants towards coastal marine ecosystems.

While reaction kinetics and redox conditions are strong precursors to these reactive hotspots, their interplay with the non-uniform velocity field and mixing dynamics in coastal aquifers remains poorly understood. Sanford and Konikow (1989) and Rezaei et al. (2005) demonstrated numerically that the mixing of salt and freshwater in coastal aquifers induces local dissolution hotspots at both the discharge zone as well as at the toe of the salt-water wedge. Studies have since also highlighted the importance of heterogeneity across the salt-freshwater interface (SFI) in generating local reaction hotspots (De Vriendt et al., 2020).

A key challenge for capturing mixing and reaction hotspots is to quantify the size of the mixing zone between freshwater and saltwater, which sets concentration gradients and thus mixing rates across the interface. Under steady-state and homogeneous conditions, mixing across the SFI is dominantly controlled by density effects and transverse dispersion (Paster & Dagan, 2007; Abarca et al., 2007). Laboratory-scale experiments (e.g., Abarca et al., 2007; Goswami & Clement, 2007; Robinson et al., 2015; Yoshihiro Oda, Tamio Takasu, Hirashi Sato, Atsushi Sawada, 2010) and some field observations (Paster et al., 2006), have shown relatively sharp mixing zones, with small widths compared to the aquifer scale. On the other hand, large-scale field studies have observed mixing zones ranging from tens to hundreds of meters (Kroeger & Charette, 2008; Spiteri et al., 2008; Kim et al., 2007; Price et al., 2003; Langevin, 2003; Barlow, 2003). Widening of the mixing zones in real-world coastal aquifers has mainly been attributed to transient effects such as tides (e.g., Ataie-Ashtiani et al., 1999; Pool et al., 2014, 2015), as well as heterogeneity (Abarca Cameo, 2006; Kerrou & Renard, 2010; Lu et al., 2013) or kinetic mass transfer (Lu et al., 2009). However, while all these investigations provide valuable insight into water-resources management and general mixing dynamics, in these studies the width of the mixing zone has been addressed mainly through averaging across and along the saltwater-freshwater interface (e.g., Abarca et al., 2007; Kerrou & Renard, 2010; Lu et al., 2013; Pool et al., 2014). Therefore, how the mixing widths vary along the interface and what are the mechanisms driving the formation of mixing and reaction hotspots are outstanding questions. Recent theoretical developments have demonstrated that fluid stretching in non-uniform flow fields can lead to increased local mixing and reactions (e.g., Le Borgne et al., 2014; Bandopadhyay et al., 2018). Here, we apply these concepts to investigate the impact of flow deformation, driven by velocity gradients in inherent to salt-freshwater interfaces, on mixing dynamics across the SFI. We quantify the evolution of the mixing width along the SFI for a range of freshwater flow rates and dispersivities and relate these dynamics to the stretching rate driven by non-homogeneous flow along the interface. We derive an approximated analytical solution which provides accurate predictions of the mixing dynamics along the SFI and allows understanding and modeling the development of mixing hotspots. We discuss the implications of our findings regarding their impact on mixing and reaction rates in coastal aquifers.

2 Methods

2.1 Flow and Transport

We study mixing under steady variable density flow in a two-dimensional cross-section of a coastal aquifer. Density-dependent flow is described by the Darcy equation

$$\mathbf{q} = -K\left(\nabla h_f + \frac{\rho - \rho_f}{\rho_f}\mathbf{e}_z\right), \tag{1}$$

where $\mathbf{q}$ is the specific discharge, K is the hydraulic conductivity, h_f the equivalent freshwater head, ρ the fluid density, ρ_f the density of freshwater and $\mathbf{e}_z$ is the unit vector in y-direction. Fluid mass conservation in the absence of sources and sinks implies $\nabla\cdot\rho\mathbf{q} = 0$. The fluid density is assumed to be linearly dependent of the salt mass fraction ω (mass of salt dissolved per unit mass of fluid) given by $\rho = \rho_f[1 + \epsilon' c]$, where ϵ' is the buoyancy factor given by $\epsilon' = (\rho_s - \rho_f)/\rho_f$ with ρ_s the density of seawater and c is the normalized salt concentration defined as $c = \omega/\omega_s$ with ω_s the salt mass fraction of seawater. The concentration c evolves according to the advection dispersion equation, which in steady state reads as

$$\mathbf{q}\cdot\nabla c - \nabla\cdot(\mathbf{D} + \phi D_m)\nabla c = 0, \tag{2}$$

with $\mathbf{D}$ the dispersion tensor (Bear, 1988), D_m molecular diffusion and ϕ porosity. We consider here a uniform hydraulic conductivity and assume that sub-scale heterogeneity is captured by the dispersivity. For this particular problem, the key dimensionless numbers that emerge are two Péclet numbers, Pe_I, which compares the advection and dispersion times, and Pe_{II}, which compares the advection and diffusion times, and the gravity number, Ng, which compares the viscous q_f/K and buoyancy forces ϵ' (see Supplementary Information) (see Abarca et al., 2007),

$$\mathsf{Pe}_I = \frac{b}{\alpha_t} \qquad \mathsf{Pe}_{II} = \frac{q_f b}{\phi D_m}. \qquad \mathsf{Ng} = \frac{K\epsilon'}{q_f}, \tag{3}$$

where b defines the domain thickness, α_t is the transverse dispersivity, q_f is the specified fresh water flux and ϕ is the porosity.

2.2 Numerical model

We consider a shallow coastal aquifer of constant thickness b and length L extended offshore with a specific freshwater discharge from inland q_f (see Figure 1a). The connection with the sea is represented as a prescribed head along the offshore model top and the offshore vertical boundaries. Different values for the fresh water flux and for the longitudinal and transverse dispersivities have been considered to evaluate their impact on mixing along the interface. The base case scenario used in this study is largely inspired from the study of Spiteri et al. (2008). However, the general relationship between fluid stretching and mixing dynamics derived from this numerical example are expected to apply more generally over a large range of coastal aquifer systems.

The values used for longitudinal and transverse dispersivities are based on typical literature values where numerical simulations were calibrated to field measurements (see table S2 in the supporting information). The values chosen for Pe_I and Pe_{II} are consistently larger than unity, as typically found in field studies and laboratory experiments (See table S2 in Supporting information). A summary of the parameters used in the numerical simulations are provided in table S1 in the supporting information. The freshwater flux ranges from $q_f = 1.25 \times 10^{-2}$ m/d to 3×10^{-2} m/d. Thus, the simulated scenarios are characterized by a Pe_I of 500, and Ng ranging between 17.3 and 7.2. Since we vary only the flow rate, the range of Ng considered is equivalent to the one of Pe_{II}. Therefore, in the following the scenarios are characterized by their Ng values. It should be noted that the gravity number in general plays a fundamental role in the movement of the wedge and has also been shown to play an important role on mixing in stable stratification problems (Dell'Oca et al., 2018).

2.3 Mixing measures

The variability of mixing along the SFI can be characterized by the local scalar dissipation rate, which is defined by

$$\chi = \nabla c \cdot \big(\mathbf{D}\nabla c\big). \tag{4}$$

For reversible mixing-limited reactions, this measure is directly proportional to the reaction rate (De Simoni, 2005). In order separate the impact of (velocity-dependent) dispersion and concentration gradient in the scalar dissipation rate, we also consider the concentration gradient,

$$\theta = \|\nabla c\|, \tag{5}$$

where $\|\cdot\|$ denotes the L^2-norm. The salt concentration gradient at the SFI can be approximated by $\theta \approx c_s/s$, where c_s is the concentration of salt in the seawater and s is the interface width. Accordingly, the evolution of the concentration gradient and thus mixing rate are determined by the interface width. The interface width is therefore a crucial element towards understanding the mixing dynamics (Paster & Dagan, 2007; Abarca et al., 2007). The width of the mixing zone normal to the principal direction of flow is determined from the width of the auxiliary function $c(1-c)$ as detailed in section 1.2 of the supporting information. All quantities are evaluated along the curvilinear length of the interface, where the toe is located at $z = 0$. We compare the scalar dissipation rate and the gradient of concentration by evaluating their local maximum values at a given depth along the length of the interface. Finally, we evaluate the rate of strain to highlight zones of enhanced fluid strain, Θ_ζ, across the interface, where flow deformation may compress the mixing zone and thus enhance concentration gradients (De Barros et al., 2012). These concepts are illustrated in Figure 1, which shows the general mixing and flow features for a salt water wedge at steady state. Figure 1a shows the setup and the definition of the mixing width.

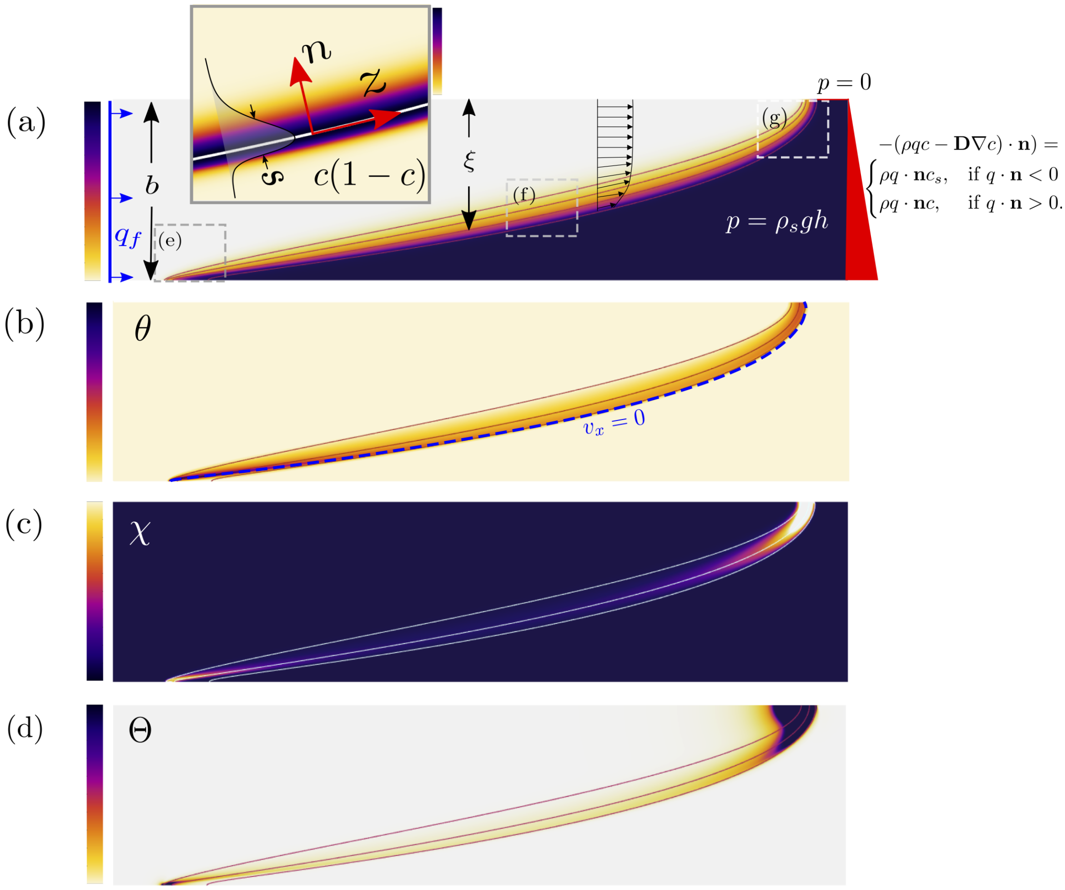

Figure 1. (a) Steady state concentration map for $\mathsf{Ng} = 17.3$. The figure illustrates the prescribed freshwater flux boundary on the left and hydrostatic head conditions on the right boundary. The inset image depicts a map of $c(1-c)$, along with a local profile of $c(1-c)$ perpendicular to the interface along the n-coordinate.(b) Map of the concentration gradient and (c) the scalar dissipation rate.

3 Mixing Mechanisms and mixing model

Figure 1b shows the evolution of the concentration gradient, which is maximum at toe and head. This evolution is also reflected in the mixing rate in Figure 1c. This behavior indicates that the width, which is inversely proportional to the concentration gradient, is small at toe and head and evolves non-monotonically in between. In order to illustrate the relation to the flow deformation, Figure 1d includes a map of the rate of strain (Okubo, 1970; Weiss, 1991; De Barros et al., 2012). These dynamics are quantified in the following by deriving an analytical model for the evolution of the mixing width in response to dispersion and flow deformation.

Mixing along the interface To investigate the impact of flow deformation on the interface width, concentration gradient and mixing rate, we vary the gravity number Ng by changing the freshwater flow rate. The local mixing widths along the interface for different Ng are shown in Figures 2(a-b). The SFI is initially narrowest at the toe where the two fluids initially mix. From here s broadens to a maximum value, s_m before narrowing again towards the discharge zone. While it has been speculated that under velocity-dependent dispersion the mixing width should increase with increasing freshwater flux (Werner et al., 2012), Figure 2a shows that the overall interface width increases for decreasing freshwater flow, i.e. increasing Ng. Figure 2b shows that all curves can be collapsed by scaling s by s_m and z by the toe length, L_t. We find that L_t grows proportional to the freshwater flux, $L_t \propto \mathsf{Ng}$ while s_m decreases as $s_m \propto \mathsf{Ng}^{1/2}$ (see Supplementary Information). Figures 2c shows the evolution of the concentration gradient θ along the interface for different Ng. All θ collapse on a single curve by when rescaled with their respective minima θ_m and plotted against z/L_t. This behavior mirrors the evolution of the mixing width as it decays from the toe toward a minimum and again increases toward the discharge. In fact, the evolution of the concentration gradient θ/θ_m can be well represented by the inverse interface width $(s/s_m)^{-1}$. We observe the same behavior for the mixing rates in Figure (2)d, which are rescaled by their minima χ_m. Their evolution is well represented by $\chi \approx \alpha_t v \theta^2$ normalized by its minimum. This highlights the central role of the interface width on mixing along the interface.

Interface mixing model The evolution of the interface width can be understood from the interplay between transverse dispersion and flow deformation. Initially, near the toe we observe enhanced mixing reflected by high concentration gradients and mixing rates. They are attributed to a local stagnation point resulting from opposing flow, which leads to enhanced interface compression. Moving away from the toe, flow velocities accelerate, which implies stretching along the interface, and at the same time interface compression perpendicular to the stretching direction. Near the toe, the compression rates are so low that transverse dispersion dominates over compression, and the interface width grows diffusively with distance as $z^{1/2}$, see Figures 2(a-b). Further up the interface, freshwater velocities increases faster due to a decrease in area between the confining unit and the interface. Eventually, at a characteristic depth z_c, the acceleration along the interface and the concurrent compression are large enough to overcome transverse dispersion. Thus, a maximum interface width is reached, followed by a succession of compression events of increasing rates that lead to a decrease of the mixing width. A similar behavior was observed by Eeman et al. (2011) when investigating up-welling of saline water across a freshwater lens into a ditch. The authors found that despite increasing velocities towards the outlet, the mixing width continued to narrow due to converging streamlines.

The competition between hydrodynamic compression and dispersive expansion can be understood more quantitatively by the following evolution equation for the mixing width s (Villermaux, 2012),

$$\frac{1}{s}\frac{ds}{dt} = -\gamma + \frac{D_t}{s^2}, \tag{6}$$

where γ is the stretching (or compression) rate and D_t/s^2 is the dispersive expansion rate with $D_t = D_m + \alpha_t v$ the transverse dispersion coefficient. The mixing time t_s, that is the time at which dispersion and compression equilibrate, is defined by $t_s = \ln(1+Pe_s)/2\gamma$ where $Pe_s = s_0^2\gamma/D_t$ (Villermaux, 2019). Although in our system, the compression rate varies along the interface, it is useful to consider the solution to Equation

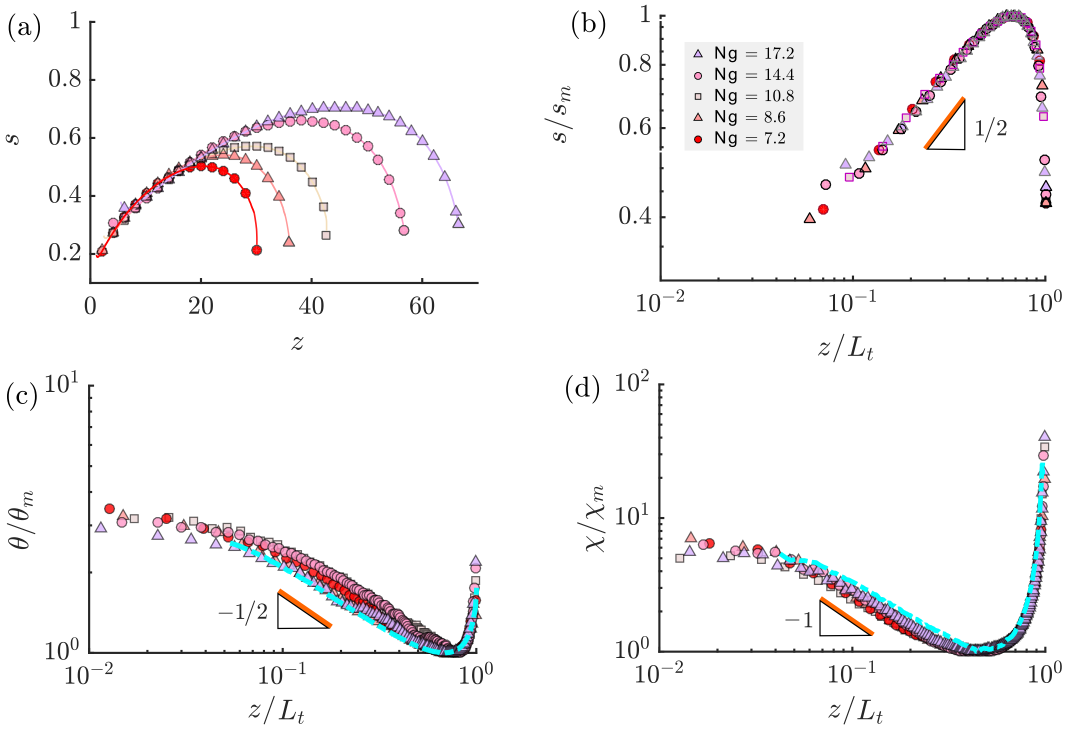

Figure 2. (a) Mixing width along the interface for (purple triangles) $\mathsf{Ng} = 17.3$, (pink circles) 14.4, (beige squares) 10.8, (light red triangles) 8.6, and (red circles)7.2. (b) Mixing widths scaled by the respective maximum interface widths s_m versus distance along the interface scaled by the toe length L_t.(c) Concentration gradients scaled by the respective minimum gradients χ_m. The blue dotted line denotes the inverse mixing width $\theta/\theta_m \approx (s/s_m)^{-1}$. (d) Scalar dissipation rates scaled by their respective minima χ_m. The dashed blue line denotes $\alpha_t v \theta^2$ normalized by its minimum.

(6) for a constant γ,

$$s = \sqrt{\frac{D_t}{\gamma}\left[1 - \exp(-2\gamma t)\right] + s_0^2 \exp(-2\gamma t)}. \tag{7}$$

For times larger than t_s, the mixing width given by Equation (7) is expected to converge to the Batchelor scale $s_B = \sqrt{D_t/\gamma}$. We define the mixing distance $z_m = v_a t_s$ as the distance over which the mixing width converges to the local Batchelor scale $s_B = \sqrt{D_t/\gamma}$. Close to the toe, $z < z_c$, the compression rate is small, which implies a large mixing distance z_m. For $z \ll z_m$, i.e. $t \ll t_s$, expression (7) behaves as $s(z) = \sqrt{D_t t} = \sqrt{\alpha_t z}$, leading to

$$s(z) = \sqrt{\alpha_t z}, \text{ for } z < z_c, \tag{8}$$

where we set the transverse dispersion coefficient $D_t \approx \alpha_t v_a$. This explains the increase of the mixing width observed in Figures 2(a-b). The dependence of s on α_t is confirmed by additional numerical simulations for variable α_t, see Supplementary Information. For increasing distance along the interface, the acceleration and thus v and γ increase notably along the interface. Assuming that v and γ change on length scales larger than the corresponding mixing distance z_m, then s evolves in a quasi-steady manner as a succession of Batchelor scales such that

$$s(z) = \sqrt{\frac{\alpha_t v(z)}{\gamma(z)}}, \text{ for } z > z_c, \tag{9}$$

where $v(z)$ and $\gamma(z)$ are the local velocity and compression rate along the interface. This second, quasi-steady regime describes the re-compression of the interface after it has reached its maximum width s_m. We notice that γ is given by the derivative of the flow velocity $v(z)$ along the interface, $\gamma(z) = dv(z)/dz$. Thus, we obtain for the interface width in terms of $v(z)$. $s(z) = \sqrt{\alpha_t \left[d \ln v(z)/dz\right]^{-1}}$ This means, the interface width can be estimated from the velocity profile. In summary, the transition between dispersive growth and compression corresponds to the crossover between two competing mechanisms. Dispersive growth is overcome by accelerating flow towards the discharge zone which stretches the interface. This leads to a compression of the mixing width in a quasi-steady manner as expressed by Eq. (9).

To derive an approximate analytical solution for the mixing width during re-compression towards the discharge zone, we must find an expression for γ. The velocity along the interface can be approximated by $v(z) = q_f b/\xi(z)$ where $\xi(z)$ is the interface height. Inserting these approximations in Equation (9), we obtain for the evolution of the interface width in the compression regime the expression

$$s(z) = \sqrt{-\alpha_t \left[\frac{d \ln \xi(z)}{dz}\right]^{-1}}, \tag{10}$$

see Supplementary Information. This means that the interface width can be estimated directly from the interface profile. In order to test this expression, we approximate the interface height by the solution of Glover (1959) as $\xi(z) = \sqrt{b^2 - 2bz/\mathsf{Ng}'}$, see Supplementary Information. Note that $\mathsf{Ng}' = \mathsf{Ng}/[1 - (\alpha_t/b)^{1/4}]$ is a modified gravity number to correct for the impact of dispersion in the interface position in the Glover solution (Pool, 2011; Lu & Werner, 2013). Inserting the expression for $\xi(z)$ into (10), we obtain the compact expression

$$s(z) = \sqrt{\alpha_t \mathsf{Ng}' b \left(1 - \frac{2z}{\mathsf{Ng}' b}\right)}. \tag{11}$$

The analytical solution explains the scaling behavior of s observed in Figure 2b. Note that the Glover solution predicts the toe length $L_t = \mathsf{Ng}' b/2$. In fact, we can write Eq. (11)

as

$$s(z) = s_m \sqrt{3\left(1 - \frac{z}{L_t}\right)}. \tag{12}$$

The cross-over position z_c between the expansion and compression regimes is obtained by matching the solution Equation (8) for the expansion regime and Equation (11) for compression. Thus, we obtain for cross-over position z_c and the maximum interface with $s_m = s(z_c)$ the explicit expressions

$$z_c = \mathsf{Ng}' b/3, \qquad s_m = \sqrt{\alpha_t z_c}. \tag{13}$$

This means that the maximum interface width and its position can be estimated from the modified gravity number and the aquifer thickness. Note that inserting z_c in the Glover solution for the interface height leads to $\xi(z_c) = b/\sqrt{(}3)$, which gives the depth above which mixing is most active due to recompression along the interface. It is interesting to note that this depth is simply a fraction of the aquifer thickness and is independent on other system properties.

Figure 3a confirms the match of the Glover solution with the interface height determined from the direct numerical simulations for different Pe_{II}. Figure 3b shows the predicted stretching rate along z together with the data from the direct numerical simulation. Note that no fitting parameter is used. Discrepancies at the toe can be attributed to local deceleration due to the stagnation zone. In addition, since the Glover solution assumes flow is forced through an infinitely small outlet rather than a gap as in the numerical simulations, γ is overestimated as it asymptotes near the outlet. Figure 3c, shows the match between the analytical expressions for the Batchelor scale and numerically derived mixing widths. Note that we multiply α_t by a factor of 3/4 to match the evolution of the data at short distance from the toe. This can be traced back to the fact that the concentration profile across the interface is not Gaussian as shown in the inset of Figure 1a. We find that the transition between dispersive growth and recompression of the interface is slightly overestimated for interfaces with small freshwater fluxes. However, in general there is good agreement between the numerical and analytical solutions. It should be emphasized that the Glover solution used in this study is a means to approximate the position and velocity along the interface for this given problem. Naturally, for problems with different boundary conditions, the interface position and and velocity field, may deviate from the idealized scenario studied here and therefore require further evaluation.

4 Conclusion

Our study has examined mixing dynamics for seawater intrusion under steady-state conditions. Evaluation of the mixing width along the salt-freshwater interface has highlighted several mixing processes that are influenced by non-uniform flow from the mixing of saline and freshwater bodies. We find that the mixing width initially grows due to transverse dispersion up to a characteristic location where it then re-compresses due to accelerating flow towards the discharge zone. Interface compression near the outlet is accompanied by enhanced concentration gradients and mixing rates. We attribute stronger mixing rates near the interface toe to enhanced local compression resulting from opposing flow which results in a stagnation point. The expansion and re-compression of the interface can be understood in terms of the flow deformation along the interface and is quantified by a mixing model that accounts for the competition of dispersive expansion and hydrodynamic compression of the interface. We show that the mixing width can be estimated from the interface profile and transverse dispersivity. Using the Glover solution for a sharp interface, we propose a simple analytical model that is capable of describing the initial growth near of the toe and its subsequent recompression near the out-

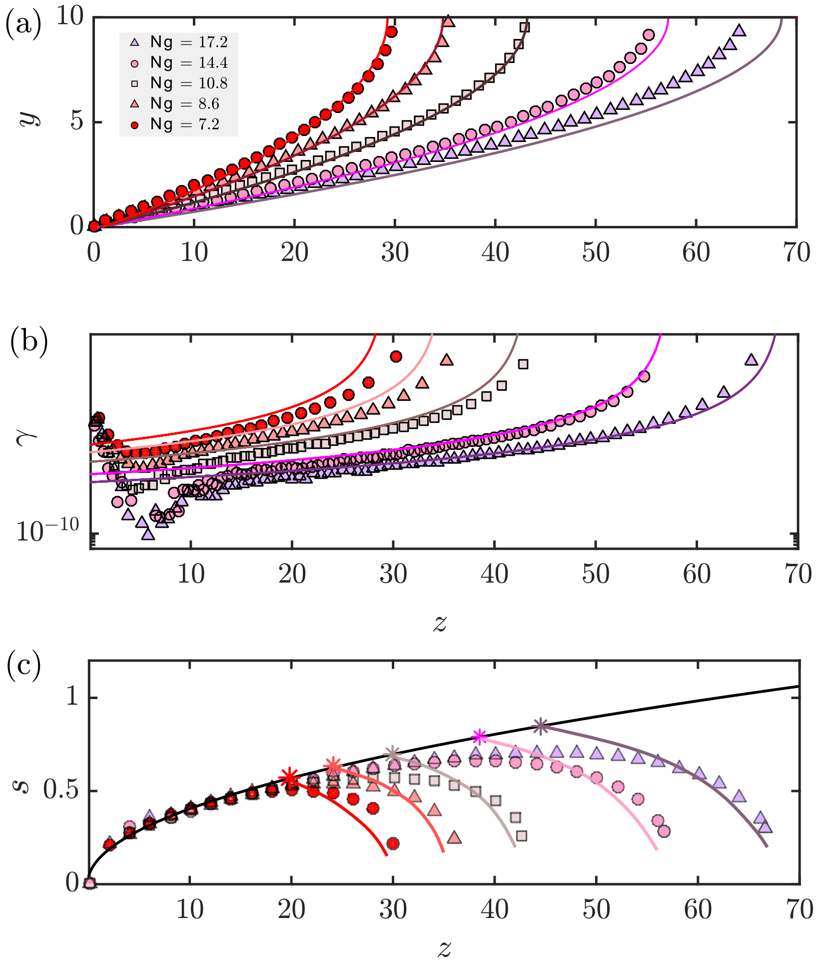

Figure 3. (a) Saltwater interface defined by the 50% concentration isoline. Symbols denote numerical simulation results and solid lines denote the Glover solutions.(b) Numerically determined Stretching rate and stretching rates determined by Glover solution (solid lines) (c) Numerical mixing width compared against the numerically derived Batchelor scale (solid lines). The solid black line denotes dispersive growth $s \sim \sqrt{z}$ prior to interface recompression. The asterisks denote the predicted the cross-over width and position.

let. While it is clear that our homogeneous model may not capture the exact mixing behavior of the SFI in more complex flow systems, e.g., in the presence of heterogeneity, 3D effects and transient forcings, it sheds light on the basic mechanisms dictating mixing across the SFI for which future work may build upon.

The mechanism leading to enhanced mixing rates across the SFI resulting from variable density induced non-uniform flow, may strongly influence our understanding of mixing-limited reactions in coastal landscapes. This is particularly relevant when evaluating the chemical composition of submarine groundwater discharge (SGD), which is often altered by biogeochemical reactions resulting from the mixing of salt and freshwater (Moore, 1999). Given that high concentrations of nutrients in coastal groundwater have been associated with eutrophication and the onset of algal blooms (Valiela et al., 1990; LaRoche et al., 1997), understanding mixing dynamics that lead to the transformation of chemicals along the interface warrants careful consideration. Our results have shown that mixing rates are intrinsically tied to the mixing evolution along the SFI (Figure 2c-d), resulting in local mixing hotspots at both the toe and head of of the interface.

Enhanced mixing at the discharge zone is of particular interest as it has been linked to an array of geochemical activity (e.g., Mylroie & Carew, 1990; Charette & Sholkovitz, 2002; Kroeger & Charette, 2008). A notable example is the precipitation of iron oxide in Waquiot Bay, USA (Charette & Sholkovitz, 2002; Spiteri et al., 2006). According to Spiteri et al. (2008), given the efficiency of iron-oxides in attenuating inorganic phosphate, these natural geochemical barriers could act to regulate nutrient dynamics prevent coastal eutrophication. It has also been shown to attenuate arsenic (Bone et al., 2006; Hun et al., 2009). Given the proximity of the discharge zone to the surface, it is also often subject to favorable redox conditions, for which the fate of groundwater nitrogen and phosphorous is highly dependent (Slomp & Cappellen, 2004). In the case of oxidative iron precipitation, a constant source of oxygen from wave and tidal action (e.g., Ullman et al., 2003; Kroeger & Charette, 2008; Charbonnier et al., 2013) in addition to enhanced mixing may explain the localization of iron oxides. It has also been suggested that even in coastal aquifers with low oxygen concentration, pH gradients across the SFI may act as the main driver in the precipitation (Spiteri et al., 2006). The non-trivial interplay between transport and chemical reactions at the discharge zone was also highlighted by Rezaei et al. (2005) in their modelling of calcite dissolution across the SFI. They emphasized that the saturation index calculation provides information of where calcite may be most undersaturated. However, it does not predict the location and magnitude of dissolution, for which spatially-resolved simulations are required. In their particular study, although calcite is always found to be most under saturated in the fresher portion of the mixing zone, dissolution was always largest along the saline portion of the discharge zone due to the active convection cell resulting in strong dispersive mixing. Our study suggests that enhanced mixing is most relevant after the cross over distance, z_c when the interface recompresses towards the discharge zone. For a salt-freshwater interface under steady state conditions, this expression may therefore provide a useful estimate towards determining where mixing enhanced reactions play an important role. From a groundwater management perspective, our study also provides a means to approximate a maximum mixing width and its location along the interface (equation 13), which may provide decision makers a straightforward method to give global estimates on the extent of salt-freshwater mixing.

Acknowledgments

This project has received funding from the European Union's Horizon 2020 research and innovation program under the Marie Sklodowska-Curie Grant Agreement No. 722028 (ENIGMA ITN). Maria Pool acknowledges the support of the Spanish Ministry of Science and Innovation through the Torres-Quevedo program (PTQ2018-010081). MD acknowledges the support of the Spanish Ministry of Science and Innovation through the project HydroPore (PID2019-106887GB-C31). Data is provided as supplementary material for the review process, and will later be deposited in a data repository with a permanent identifier.

References

Abarca, E., Carrera, J., Sánchez-Vila, X., & Dentz, M. (2007). Anisotropic dispersive Henry problem. *Advances in Water Resources*, *30*(4), 913–926. doi: 10.1016/j.advwatres.2006.08.005

Abarca Cameo, E. (2006). *Seawater intrusion in complex geological environments* (Unpublished doctoral dissertation). Technical University of Catalonia, UPC.

Ataie-Ashtiani, B., Volker, R. E., & Lockington, D. A. (1999). Tidal effects on sea water intrusion in unconfined aquifers. *Journal of Hydrology*, *216*(1-2), 17–31. doi: 10.1016/S0022-1694(98)00275-3

Back, W., Hanshaw, B. B., Pyle, T. E., Plummer, L. N., & Weidie, A. E. (1979). Geochemical significance of groundwater discharge and carbonate solution to the formation of Caleta Xel Ha, Quintana Roo, Mexico. *Water Resources Research*, *15*(6), 1521–1535. doi: 10.1029/WR015i006p01521

Back, W., Hanshaw, B. B., Survey, U. S. G., Herman, J. S., Sciences, E., Driel, J. N. V., & Survey, U. S. G. (1986a). Differential dissolution of a Pleistocene reef in the ground-water mixing zone of coastal Yucatan , Mexico. *Geology*, *14*(February), 137–140.

Back, W., Hanshaw, B. B., Survey, U. S. G., Herman, J. S., Sciences, E., Driel, J. N. V., & Survey, U. S. G. (1986b). Differential dissolution of a Pleistocene reef in the ground-water mixing zone of coastal Yucatan , Mexico. (February), 137–140.

Bandopadhyay, A., Davy, P., & Borgne, T. L. (2018). Shear Flows Accelerate Mixing Dynamics in Hyporheic Zones and Hillslopes. *Geophysical Research Letters*, 659–668. doi: 10.1029/2018GL079914

Barlow, P. M. (2003). *Ground Water in Freshwater-Saltwater Environments of the Atlantic Coast* (Tech. Rep.). Geological Survey (USGS).

Bear, J. (1988). *Dynamics of fluids in porous media.* Dover publications, inc New York.

Bone, S. E., Gonneea, M., & Charette, M. A. (2006). Geochemical cycling of arsenic in a coastal aquifer. *Environmental Science and Technology*, 3273–3278.

Charbonnier, C., Anschutz, P., Poirier, D., Bujan, S., & Lecroart, P. (2013). Aerobic respiration in a high-energy sandy beach. *Marine Chemistry*, *155*, 10–21. Retrieved from `http://dx.doi.org/10.1016/j.marchem.2013.05.003` doi: 10.1016/j.marchem.2013.05.003

Charette, M. A., & Sholkovitz, E. R. (2002). Oxidative precipitation of groundwater-derived ferrous iron in the subterranean estuary of a coastal bay. *Geophysical Research Letters*, *29*(10), 85–1–85–4. doi: 10.1029/2001gl014512

De Barros, F. P. J., Dentz, M., Koch, J., & Nowak, W. (2012). Flow topology and scalar mixing in spatially heterogeneous flow fields. *Geophysical Research Letters*, *39*(8), 1–5. doi: 10.1029/2012GL051302

De Simoni, M. (2005). A procedure for the solution of multicomponent reactive transport problems. , *41*, 1–16. doi: 10.1029/2005WR004056

De Vriendt, K., Pool, M., & Dentz, M. (2020). Heterogeneity-Induced Mixing and Reaction Hot Spots Facilitate Karst Propagation in Coastal Aquifers. *Geophysical Research Letters*, *47*(10), 1–12. doi: 10.1029/2020GL087529

Dell'Oca, A., Riva, M., Carrera, J., & Guadagnini, A. (2018). Solute dispersion for stable density-driven flow in randomly heterogeneous porous media. *Advances in Water Resources*, *111*(April 2017), 329–345. Retrieved from `https://doi.org/10.1016/j.advwatres.2017.10.040` doi: 10.1016/j.advwatres.2017.10.040

Eeman, S., Leijnse, A., Raats, P. A., & van der Zee, S. E. (2011). Analysis of the thickness of a fresh water lens and of the transition zone between this lens and upwelling saline water. *Advances in Water Resources*, *34*(2), 291–302. Retrieved from http://dx.doi.org/10.1016/j.advwatres.2010.12.001 doi: 10.1016/j.advwatres.2010.12.001

Ferguson, G., & Gleeson, T. (2012). Vulnerability of coastal aquifers to groundwater use and climate change. *Nature Climate Change*, *2*(5), 342–345. Retrieved from http://dx.doi.org/10.1038/nclimate1413 doi: 10.1038/nclimate1413

Glover, R. E. (1959). The pattern of fresh-water flow in a coastal aquifer. *Journal of Geophysical Research*, *64*(4), 457–459. doi: 10.1029/jz064i004p00457

Goswami, R. R., & Clement, T. P. (2007). Laboratory-scale investigation of saltwater intrusion dynamics. *Water Resources Research*, *43*(4), 1–11. doi: 10.1029/2006WR005151

Hun, B. J., Charette, M. A., & Zheng, Y. (2009). Field, laboratory, and modeling study of reactive transport of groundwater arsenic in a coastal aquifer. *Environmental Science and Technology*, *43*(14), 5333–5338. doi: 10.1021/es900080q

Kerrou, J., & Renard, P. (2010). A numerical analysis of dimensionality and heterogeneity effects on advective dispersive seawater intrusion processes. *Hydrogeology Journal*, *18*(1), 55–72. doi: 10.1007/s10040-009-0533-0

Kim, K.-y., Chon, C.-m., & Park, K.-h. (2007). A Simple Method for Locating the Fresh Water – Salt Water Interface Using Pressure Data. *Ground Water*, *45*(6), 723–728. doi: 10.1111/j.1745-6584.2007.00349.x

Kroeger, K. D., & Charette, M. A. (2008). Nitrogen biogeochemistry of submarine groundwater discharge. *Limnology and Oceanography*, *53*(3), 1025–1039. doi: 10.4319/lo.2008.53.3.1025

Langevin, C. D. (2003). Simulation of Submarine Ground Water Discharge to a Marine Estuary : Biscayne Bay , Florida. *Ground Water*, *41*(6), 758–771.

LaRoche, J., Nuzzi, R., Waters, R., Wyman, K., Falkowski, P., & Wallace, D. (1997). Brown Tide blooms in Long Island ' s coastal waters linked to interannual variability in groundwater flow. *Global Change Biology*, *3*(5), 397–410.

Le Borgne, T., Ginn, T. R., & Dentz, M. (2014). Impact of fluid deformation on mixing-induced chemical reactions in heterogeneous flows. *Geophysical Research Letters*, *41*(22), 7898–7906. doi: 10.1002/2014GL062038

Lu, C., Chem, Y., Zhang, C., & Luo, J. (2013). Steady-state freshwater–seawater mixing zone in stratified coastal aquifers. *Journal of Hydrology*, *9*. Retrieved from http://www.tandfonline.com/doi/abs/10.1080/18146627.2012.755281 doi: 10.1016/j.jhydrol.2013.09.017

Lu, C., Kitanidis, P. K., & Luo, J. (2009). Effects of kinetic mass transfer and transient flow conditions on widening mixing zones in coastal aquifers. *Water Resources Research*, *45*(December 2008), 1–17. doi: 10.1029/2008WR007643

Lu, C., & Werner, A. D. (2013). Advances in Water Resources Timescales of seawater intrusion and retreat. *Advances in Water Resources*, *59*, 39–51. Retrieved from http://dx.doi.org/10.1016/j.advwatres.2013.05.005 doi: 10.1016/j.advwatres.2013.05.005

Moore, W. S. (1999). The subterranean estuary: A reaction zone of ground water and sea water. *Marine Chemistry*, *65*(1-2), 111–125. doi: 10.1016/S0304-4203(99)00014-6

Moore, W. S. (2010). A reevaluation of submarine groundwater discharge along the southeastern coast of North America. , *24*(December 2009), 1–9. doi: 10.1029/2009GB003747

Mylroie, J. E., & Carew, J. L. (1990). The flank margin model for dissolution cave development in carbonate platforms. *Earth Surface Processes and Landforms*, *15*, 413–424.

Okubo, A. (1970). Horizontal dispersion of floatable particles in the vicinity of velocity singularities such as convergences. *Deep-Sea Research and Oceanographic Abstracts*, *17*(3), 445–454. doi: 10.1016/0011-7471(70)90059-8

Palmer, A. (1992). Origin and morphology of limestone caves. *Geological Society of America Bulletin*, *103*(January 1991), 1–21.

Palmer, R., & Williams, D. (1982). Cave development under Andros Island, Bahamas. *Cave Science*, *11*(1), 50–52.

Paster, A., & Dagan, G. (2007). Mixing at the interface between two fluids in porous media: a boundary-layer solution. *Journal of Fluid Mechanics*, *584*, 455–472. doi: 10.1017/S0022112007006532

Paster, A., Dagan, G., & Guttman, J. (2006). The salt-water body in the Northern part of Yarkon-Taninim aquifer : Field data analysis , conceptual model and prediction. *Journal of Hydrology*, *323*, 154–167. doi: 10.1016/j.jhydrol.2005.08.018

Pool, M. (2011). *Simplified approaches to deal with the complexities of Seawater Intrusion* (Unpublished doctoral dissertation).

Pool, M., Post, V. E., & Simmons, C. T. (2014). aquifers : Homogeneous case. *Water Resources Research*, 6910–6926. doi: 10.1002/2014WR015534.Received

Pool, M., Post, V. E. A., & Simmons, C. T. (2015). Effects of tidal fluctuations and spatial heterogeneity on mixing and spreading in spatially heterogeneous coastal aquifers. , 1570–1585. doi: 10.1002/2014WR016068.Received

Price, R. M., Top, Z., Happell, J. D., & Swart, P. K. (2003). Use of tritium and helium to define groundwater flow conditions in Everglades National Park. *Water Resources Research*, *39*(9), 1–12. doi: 10.1029/2002WR001929

Rezaei, M., Sanz, E., Raeisi, E., & Ayora, C. (2005). Reactive transport modeling of calcite dissolution in the fresh-salt water mixing zone. *Journal of Hydrology*, *311*, 282–298. doi: 10.1016/j.jhydrol.2004.12.017

Robinson, G., Hamill, G. A., & Ahmed, A. A. (2015). Automated image analysis for experimental investigations of salt water intrusion in coastal aquifers. *Journal of Hydrology*, *530*, 350–360. Retrieved from `http://dx.doi.org/10.1016/j.jhydrol.2015.09.046` doi: 10.1016/j.jhydrol.2015.09.046

Sanford, W. E., & Konikow, L. F. (1989). Simulation of Calcite Dissolution and Porosity Changes in Saltwater Mixing Zones in Coastal Aquifers. *Water Resources Research*, *25*(4), 655–667.

Slomp, C. P., & Cappellen, P. V. (2004). Nutrient inputs to the coastal ocean through submarine groundwater discharge : controls and potential impact. *Journal of Hydrology*, *295*, 64–86. doi: 10.1016/j.jhydrol.2004.02.018

Spiteri, C., Regnier, P., Slomp, C. P., & Charette, M. A. (2006). pH-Dependent iron oxide precipitation in a subterranean estuary. *Journal of Geochemical Exploration*, *88*(1-3 SPEC. ISS.), 399–403. doi: 10.1016/j.gexplo.2005.08.084

Spiteri, C., Slomp, C. P., Charette, M. A., Tuncay, K., & Meile, C. (2008). Flow and nutrient dynamics in a subterranean estuary (Waquoit Bay , MA , USA): Field data and reactive transport modeling. *Geochimica et Cosmochimica Acta*, *72*(3), 3398–3412. doi: 10.1016/j.gca.2008.04.027

Ullman, W. J., Chang, B., Miller, D. C., & Madsen, J. A. (2003). Groundwater mixing, nutrient diagenesis, and discharges across a sandy beachface, Cape Henlopen, Delaware (USA). *Estuarine, Coastal and Shelf Science*, *57*(3), 539–552. doi: 10.1016/S0272-7714(02)00398-0

Valiela, I., Costa, J., Foreman, K., Teal, J. M., Howes, B., & Aubrey, D. (1990). Transport of groundwater-borne nutrients from watersheds and their effects on coastal waters. *Biogeochemistry*, *10*(7418), 177–197.

Villermaux, E. (2012). Mixing by porous media. *Comptes Rendus - Mecanique*, *340*(11-12), 933–943. Retrieved from `http://dx.doi.org/10.1016/j.crme.2012.10.042` doi: 10.1016/j.crme.2012.10.042

Villermaux, E. (2019). Mixing Versus Stirring. (August 2018), 245–273.

Weiss, J. (1991). The dynamics of enstrophy transfer in two-dimensional hydrodynamics. *Physica D: Nonlinear Phenomena*, *48*(2-3), 273–294. doi: 10.1016/0167-2789(91)90088-Q

Werner, A. D., Bakker, M., Post, V. E. A., Vandenbohede, A., Lu, C., Ataie-ashtiani, B., ... Barry, D. A. (2012). Seawater intrusion processes, investigation and management: Recent advances and future challenges. *Advances in Water Resources*. Retrieved from `http://dx.doi.org/10.1016/j.advwatres.2012.03.004` doi: 10.1016/j.advwatres.2012.03.004

Yoshihiro Oda, Tamio Takasu, Hirashi Sato, Atsushi Sawada, T. W. (2010). Optical measurement of the salinity distribution by saltwater intrusion experiment. *Japan Society of Civil Engineers*, *67*(2), 186–197.

Supporting Information for "Subsurface Mixing Dynamics across the Salt-freshwater Interface"

K.De Vriendt[1], T.Le Borgne[2], M.Pool[3], M.Dentz[1]

[1]IDAEA-CSIC,Institute of Environmental Assessment and Water Research, Spanish National Research Institute

[2]Universit de Rennes 1, CNRS, Gosciences Rennes UMR 6118, Rennes, France

[3]AMPHOS 21 Consulting S. L., 08019 Barcelona

[1]18 26, Calle Jordi Girona, 18-26, 08034 Barcelona

1. Model Parameters

Values of parameters used in the numerical simulations are provided in table S1.

1.1. Dispersivities

Numerical studies have shown that the longitudinal and transverse dispersivities α_l and α_t are important parameters when considering mixing dynamics and the width of the SFI (e.g. Abarca et al., 2007; Nick et al., 2013; Spiteri et al., 2008). Unlike the evolution of plumes over time, there exists no clear criterion for assigning the value of dispersivities (Rezaei et al., 2005). This is further confounded by the fact that it is a parameter that is generally difficult to measure and is scale dependent (Neuman, 1990). Numerical studies of field sites often adopt arbitrarily large dispersivity values in order to overcome numerical dispersion caused by poor grid refinement in numerical codes (Paster, 2010), or to artificially incorporate the effects of tides and heterogeneity (Werner et al., 2012). However, large dispersion likely lead to an overestimation of mixing induced reaction rates.

In Figure S2, we see that increasing α_l has negligible impact on the overall mixing width compared to α_t. For example, increasing α_l by a factor of 5 for $\alpha_t = 0.01$ m, results in almost no change in s_m. This is not surprising given the bulk of the interface resides where flow is tangential to the principal direction of flow. Flow from the seaside however approaches the interface orthogonally with velocities approximately an order of magnitude lower than the freshwater flux. This, however is by no means suggesting α_l play no role in the behaviour of the mixing zone. Abarca et al. (2007) showed that increasing α_l leads to the seaward displacement of high concentration isolines, with a particularly strong influence at toe. Therefore for larger values of α_l, the analytical solution may no longer provide provide a good fit. For smaller dispersivities however, which are in-line with literature values seen in table S2, α_t alone seems to sufficiently characterizes the growth of s.

2. Mixing width

To determine the mixing width, we compute the distance across $c(1 - c)$ at half its maximum, denoted here as κ. Due to the proximity of the toe to boundary, the full width at half maximum cannot be attained directly at the bottom and are omitted. For a symmetric profile of $c(1 - c)$, we can relate this back to the square root of the second central moment (variance) of $c(1 - c)$,

$$s = \frac{\kappa}{2\sqrt{2\ln 2}}, \tag{1}$$

where s defines the mixing width.

3. Interface width and interface height

We first recall that the stretching rate is defined by

$$\gamma(z) = \frac{dv(z)}{dz}. \tag{2}$$

Inserting this expression into expression (8) in the main text for $s(z)$, we can write

$$s(z) = \sqrt{\alpha_t \left[\frac{d\ln v(z)}{dz}\right]^{-1}}. \tag{3}$$

We estimate the velocity along the interface from volume conservation and set

$$v(z) = \frac{q_f b}{\xi(z)}, \tag{4}$$

where $\xi(z)$ is the interface height that is $\xi(z=0) = b$ at the toe postion at $z = 0$ and 0 at the outflow. With this definition, we obtain for the interface width in Eq. (3)

$$s(z) = \sqrt{-\alpha_t \left[\frac{d\ln \xi(z)}{dz}\right]^{-1}}. \tag{5}$$

4. Interface width from the Glover solution

To derive an approximation for the mixing width in the compression regime, we consider the sharp interface solution of Glover (1959) that predicts the position of the interface as,

$$\xi^2 = \frac{2Q_f}{K\epsilon'} z + \frac{Q_f^2}{K^2\epsilon'^2}, \tag{6}$$

where $Q_f = q_f b$, recalling q_f is the freshwater flux and b is the domain height. To account for the influence of mixing we incorporate the empirical correction factor for the buoyancy factor, ϵ', as introduced by Pool (2011),

$$\epsilon = \epsilon' \left[1 - \left(\frac{\alpha_t}{b} \right)^{1/4} \right]^{-1}. \tag{7}$$

We implement the factor 1/4 suggested by (Lu & Werner, 2013) as it provides a better fit against the numerical simulations. We transform equation (6) such that $z = 0$ coincides with the toe position. Thus, we obtain

$$\xi = \sqrt{b^2 - \frac{2b}{\mathsf{Ng}'} z}, \tag{8}$$

where we defined the modified gravity number, $\mathsf{Ng}' = K\epsilon/q_f$. Note that $\xi(z = 0) = b$. The the length of the toe is predicted by the Glover solution as

$$L_t = \frac{b\mathsf{Ng}'}{2}. \tag{9}$$

Inserting (8) into (5), we obtain for the interface width during the compression regime the explicit expression

$$s(z) = \sqrt{\alpha_t(\mathsf{Ng}'b - 2z)}. \tag{10}$$

References

Abarca, E., Carrera, J., Sánchez-Vila, X., & Dentz, M. (2007). Anisotropic dispersive Henry problem. *Advances in Water Resources*, *30*(4), 913–926. doi: 10.1016/j.advwatres.2006.08.005

Abarca, E., & Clement, T. P. (2009). A novel approach for characterizing the mixing zone of a saltwater wedge. *Geophysical Research Letters*, *36*(January), 1–5. doi: 10.1029/2008GL036995

Abarca, E., Karam, H., Hemond, H. F., & Harvey, C. F. (2013). Transient groundwater dynamics in a coastal aquifer : The effects of tides , the lunar cycle , and the beach profile. *Water Resources Research*, *49*(May), 2473–2488. doi: 10.1002/wrcr.20075

Glover, R. E. (1959). The pattern of fresh-water flow in a coastal aquifer. *Journal of Geophysical Research*, *64*(4), 457–459. doi: 10.1029/jz064i004p00457

Heiss, J. W., & Michael, H. A. (2014). This Copy of a Work Protected By Canadian Copyright Law Is To. *Water Resources Research*, 6747–6766. doi: 10.1002/2014WR015574.Received

Lu, C., & Werner, A. D. (2013). Advances in Water Resources Timescales of seawater intrusion and retreat. *Advances in Water Resources*, *59*, 39–51. Retrieved from `http://dx.doi.org/10.1016/j.advwatres.2013.05.005` doi: 10.1016/j.advwatres.2013.05.005

Masahiro, T., Momii, K., & Luyun Jr, R. (2018). Laboratory Scale Investigation of Dispersion Effects on Saltwater Movement due to Curoff Wall Installation. In *25th salt water intrusion meeting* (pp. 323–328). Gdansk.

Neuman, P. (1990). Universal scaling of hydraulic conductivities and dispersivities in geologic media. *Water Resources Research*, *26*(8), 1749–1758.

Nick, H. M., Raoof, A., Centler, F., Thullner, M., & Regnier, P. (2013). Reactive dispersive contaminant transport in coastal aquifers : Numerical simulation of a reactive Henry problem. *Journal of Contaminant Hydrology*, *145*, 90–104. Retrieved from `http://dx.doi.org/10.1016/j.jconhyd.2012.12.005` doi: 10.1016/j.jconhyd.2012.12.005

Paster, A. (2010). Mixing between fresh and salt waters at aquifer regional scale and identification of transverse dispersivity. *Journal of Hydrology*, *380*(1-2), 36–44. Retrieved from http://dx.doi.org/10.1016/j.jhydrol.2009.10.018 doi: 10.1016/j.jhydrol.2009.10.018

Pool, M. (2011). *Simplified approaches to deal with the complexities of Seawater Intrusion* (Unpublished doctoral dissertation).

Rezaei, M., Sanz, E., Raeisi, E., & Ayora, C. (2005). Reactive transport modeling of calcite dissolution in the fresh-salt water mixing zone. *Journal of Hydrology*, *311*, 282–298. doi: 10.1016/j.jhydrol.2004.12.017

Robinson, C., Gibbes, B., Carey, H., & Li, L. (2007). Salt-freshwater dynamics in a subterranean estuary over a spring-neap tidal cycle. *Journal of Geophysical Research*, *112*(June), 1–15. doi: 10.1029/2006JC003888

Robinson, G., Hamill, G. A., & Ahmed, A. A. (2015). Automated image analysis for experimental investigations of salt water intrusion in coastal aquifers. *Journal of Hydrology*, *530*, 350–360. Retrieved from http://dx.doi.org/10.1016/j.jhydrol.2015.09.046 doi: 10.1016/j.jhydrol.2015.09.046

Spiteri, C., Slomp, C. P., Tuncay, K., & Meile, C. (2008). Modeling biogeochemical processes in subterranean estuaries : Effect of flow dynamics and redox conditions on submarine groundwater discharge of nutrients. *Water Resources Research*, *44*, 1–18. doi: 10.1029/2007WR006071

Werner, A. D., Bakker, M., Post, V. E. A., Vandenbohede, A., Lu, C., Ataie-ashtiani, B., ... Barry, D. A. (2012). Seawater intrusion processes, investigation and management: Recent advances and future challenges. *Advances in Water Re-*

sources. Retrieved from http://dx.doi.org/10.1016/j.advwatres.2012.03.004 doi: 10.1016/j.advwatres.2012.03.004

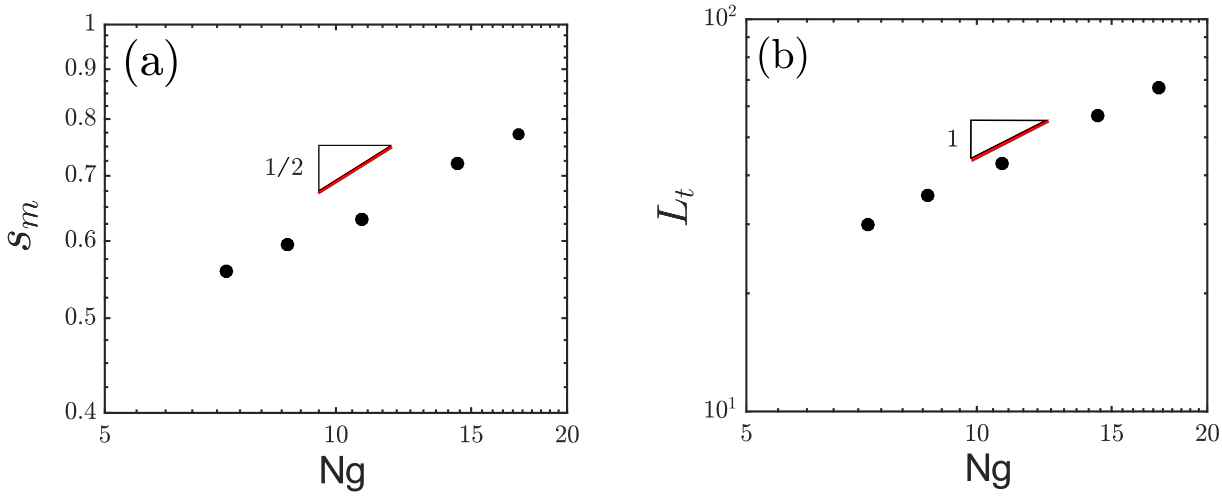

Figure S1. a) Maximum mixing width, s_m and the b) toe length, L_t obtained from numerical models as a function of Ng

Table S1. Parameters used in numerical simulations

Parameter	Value	Description
$K[ms^{-1}]$	1 x 10^{-4}	Hydraulic conductivity
$b[m]$	10	Aquifer thickness
$L[m]$	100	Aquifer Length
$\phi[-]$	0.3	Porosity
$\alpha_l[m]$	0.2	Longitudinal dispersivity
$\alpha_t[m]$	0.02	Transverse dispersivity
$q_f[md^{-1}]$	0.0125, 0.015, 0.02, 0.025 and 0.03	Freshwater flux
$\mathsf{Ng}[-]$	17.3, 14.4, 10.8, 8.6 and 7.2	Freshwater flux
$D_m\ [m^2/s]$	1e-9	Molecular diffusion
$\epsilon'[-]$	0.025	Buoyancy factor

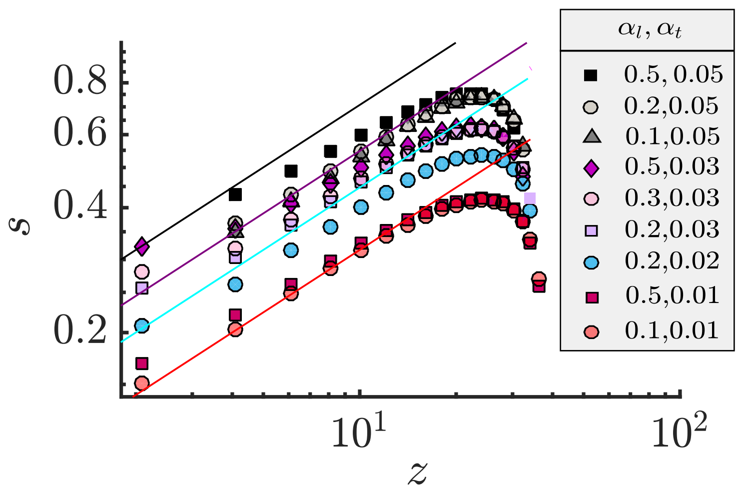

Figure S2. Mixing width for varying dispersivities. Solid lines indicate interface growth for the numerical transverse dispersivity.

Table S2. Literature derived values of coastal aquifer properties

Publication	**Type**	K [m/s]	q_f [m/d]	b [m]	α_l (m)	α_t (m)
Paster (2010)	Field	1.73 x 10^{-3}	-	600-1000	-	0.04
Abarca et al. (2013)	Field	1.74 x 10^{-4}	2.3 x 10^{-2}	11	0.1	0.01
Heiss and Michael (2014)	Field	2.9 x 10^{-4}	-	12-18	0.15	1.5 x 10^{-2}
Spiteri et al. (2008)	Field	6.86 x 10^{-4}	0.13	11	0.5	5 x 10^{-3}
C. Robinson et al. (2007)	Field	1.16 x 10^{-4}	6.6 x 10^{-2}	30	0.5	5 x 10^{-2}
Abarca and Clement (2009)	Experimental	1.2 x 10^{-2}	-	0.3	5 x 10^{-4}	5 x 10^{-5}
G. Robinson et al. (2015)	Experimental	2.3 x 10^{-3}	-	0.14	1 x 10^{-3}	5 x 10^{-4}
Masahiro et al. (2018)	Experimental	-	-	0.25	7 x 10^{-4}	2.5 x 10^{-5}

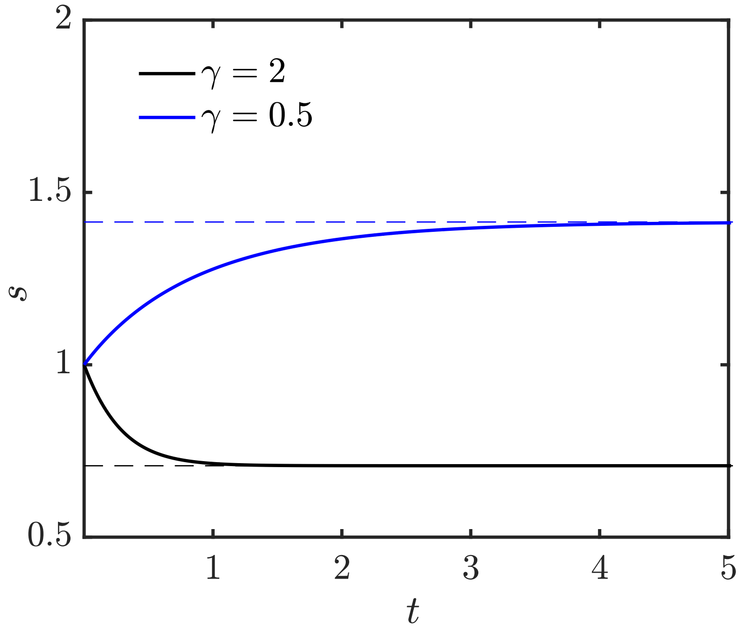

Figure S3. Evolution of mixing width given two different stretching rates. Blue line shows diffusive growth of an interface towards a large bachelor scale (blue dashed line) given a small stretching rate whereas the black line shows the mixing width compressing exponentially towards a small Batchelor scale (black dashed line)